String Flash-Boiling in Flashing and Non-Flashing Gasoline Direct Injection Simulations with Transient Needle Motion

E.T. Baldwin[1*], R.O. Grover, Jr[2], D.J. Duke[3], K.E. Matusik[3], A.L. Kastengren[4], C.F. Powell[3], S.E. Parrish[2] and D.P. Schmidt[1]

[1]University of Massachusetts Amherst
[2]General Motors Research and Development
[3]Energy Systems Division, Argonne National Laboratory, Lemont IL USA 60439
[4]X-ray Science Division, Argonne National Laboratory, Lemont IL USA 60439

Abstract

A computational study was performed to investigate the influence of transient needle motion on gasoline direct injection (GDI) internal nozzle flow and near-field sprays. Simulations were conducted with a compressible Eulerian flow solver modeling liquid, vapor, and non-condensable gas phases with a diffuse interface. Variable rate generation and condensation of fuel vapor were captured using the homogeneous relaxation model (HRM). The non-flashing (spray G) and flashing (spray G2) conditions specified by the Engine Combustion Network were modeled using the nominal spray G nozzle geometry and transient needle lift and wobble were based upon ensemble averaged x-ray imaging preformed at Argonne National Lab. The minimum needle lift simulated was 5 μm and dynamic mesh motion was achieved with Laplacian smoothing. The results were qualitatively validated against experimental imaging and the experimental rate of injection profile was captured accurately using pressure boundary conditions and needle motion to actuate the injection. Needle wobble was found to have no measurable effect on the flow. Low needle lift is shown to result in vapor generation as fuel rushes past the needle. And finally, the internal injector flow is shown to contain many transient and interacting vortices which cause perturbations in the spray angle, fluctuations in the mass flux, and frequently result in string flash-boiling.

*Corresponding Author: ebaldwin@umass.edu

Introduction

In recent years there has been a trend in the automotive industry towards the use of gasoline direct injection (GDI) engines. This injection configuration allows for more control over the combustion process, which leads to increased fuel economy. While GDI engines have developed significantly since their inception, there is still work to be done. The desire to further reduce emissions and maximize fuel efficiency demand continued improvement.

The injection process is very important because it is the first step in the combustion process. Here high pressure fuel flows though the injector and sprays directly into the combustion chamber. The complexity of this process is due to multiple factors. First, the geometries of GDI injectors are typically quite elaborate; multi-hole valve covered orifice (VCO) injectors with counterbored nozzles are common. This, in conjunction with the high injection pressures, leads to turbulent flows which often exhibit slight asymmetry and hole-to-hole variation as they leave the nozzle [1, 2]. Furthermore, as the liquid fuel is injected it can undergo phase change through cavitation, flash-boiling, and/or evaporation. Significant research has been done to understand the highly turbulent, cavitating, and evaporating sprays present in direct injection (DI) diesel engines, and while there is some overlap between diesel DI and GDI, it is the added factor of phase change through flash-boiling that makes GDI research especially challenging.

The process of vapor generation is highly complex. Vaporization takes place at small length scales and is influenced by the complex interfacial and turbulent dynamics of the flow. Moreover, phase change occurs at different rates depending on the properties of the flow. The vapor pressure and vapor density of a cold fluid is typically very low. Because of this, less heat transfer is required per volume of vapor, and cavitation, which occurs at low temperatures, tends to occur quickly. On the other hand, the vapor density of a hot liquid is much higher. Consequently, more heat transfer is required per volume of vapor and flash-boiling tends to generate vapor at a slower rate. This can be understood further with the help of the non-dimensional Jakob number which is the ratio of the sensible heat available to the latent heat required for vaporization [3].

$$Ja = \frac{\rho_l C_p \Delta T}{\rho_v h_{fg}} \tag{1}$$

Here ρ_l is the liquid density, ρ_v is the vapor density, C_p is the specific heat at constant pressure, ΔT is the degree of superheat, and h_{fg} is the enthalpy of vaporization. When the Jakob number is high there will be an abundance of energy available in the liquid to generate vapor. This means that heat transfer time scales will be much smaller than flow time scales and it can be assumed that the flow is at thermal equilibrium. Alternatively, when the Jakob number is low, heat transfer time scales will be of the same order as that of the flow and thermal equilibrium cannot be assumed.

In a modern GDI engine, a wide range of Jakob numbers can be present. This is due to the wide range of operating conditions that an engine will encounter. Fuel temperatures can vary from below zero during a cold start on a winter day, to upwards of 90°C under high engine load. In-cylinder temperature and pressure can also vary significantly depending on whether injection occurs early during the intake stroke for homogeneous combustion, or late in the compression stroke for stratified, highly lean local combustion. Depending on the combination of fuel temperature and downstream pressure, the degree to which the spray is flash-boiling will vary. This means that GDI engines must be designed to utilize hard flashing, moderately flashing, and sub cooled sprays.

A multitude of experimental studies have attempted to characterize the behavior of flash-boiling sprays. Among them, it is commonly observed that the spray structure is completely altered by flash-boiling conditions; penetration is reduced, atomization and spray angle are increased, and often a large recirculating toroidal vortex is present around the tip of the jet [4–6]. Compared to non-flashing conditions, where the Weber number and Reynolds number are highly important [7], under flashing conditions Zeng et al. [8] and Xu et al [6] have shown that it is the ambient to saturated pressure ratio (P_a/P_s) which correlates well with spray characteristics.

Experimental studies done on multi-hole injectors commonly observe a collapse of the spray under hard flashing conditions [8–14]. This collapse typically occurs at or below (P_a/P_s) of 0.3 as the quickly expanding spray plumes interact with one another [8]. The collapse of these sprays alters the designed directionality of the injectors and inhibits mixing with the ambient gas. Hole-to-hole variation in mass flow rate [1] and spray plume structure [2] is also commonly observed. In such cases, it is possible factors such as asymmetry in the nozzle geometry and the manufacturing defects work together to generate asymmetry in the flow.

Many experimental studies describe their observations with semi-empirical zero or one-dimensional models [5–7, 15, 16]. These are beneficial to an ex-

tent, however, they will never be able to represent the sprays generated by the complex geometries present in production injectors. For example, consider the significant influence manufacturing imperfections can have on sprays; Kastengren et al. observed differences in sprays from nominally identical injectors [17], and Zhang et al. observed differences in GDI sprays from nominally identical injectors which were fabricated with different techniques [18]. The significant influence of such subtle differences are beyond the scope of lower order models, however CFD can capture these effects [19]. For this reason, CFD simulations have an important role to play, both as an engineering design tool and in the academic investigation into the complex physics occurring within these sprays.

Eulerian CFD spray models have become increasingly popular in recent years. These models have the benefit of easily capturing the internal nozzle flow and external spray in a single simulation. Depending on how the model is designed to handle the multiphase interface it can either be classified as a sharp interface or a diffuse interface model.

Sharp interface models use a variety of numerical techniques to attempt to maintain and reconstruct the interface. This approach is appealing because it relies on first principles and the interfacial effects are directly simulated. These models are a beneficial tool in helping to understand the underlying mechanisms which determine a nozzle's spray characteristics. For example Shost et al. [20] and Befrui et al. [21] used a VOF-LES model to simulate GDI sprays and elucidate the influence of nozzle geometry, flow turbulence, and aerodynamic instabilities on GDI sprays.

Unfortunately, this approach faces two significant drawbacks when applied to spray modeling. First, it can be prohibitively expensive as it requires that the interface be fully resolved. While this is possible for some lower pressure GDI sprays, the high Reynolds and Weber numbers present in most diesel and some GDI sprays render this approach extremely expensive. Furthermore, the expense is compounded significantly in flash-boiling conditions where very small bubbles can be present within the spray itself, rendering the interface extremely complex. Second, this approach is inappropriate all together when a sharp interface is not physically present, for instance in diesel sprays which can be near-supercritical [22, 23].

Alternatively, the diffuse interface approach attempts to model the behavior of the interface rather than resolve it. These types of models have been extremely successful in simulating diesel sprays [24–30], and recently they have been applied to GDI sprays by Moulai et al. [31], Saha et al. [32], and Strek et al. [1]. These three works all similarly modeled GDI internal nozzle flow and near field flashing and non-flashing spray through the spray G Engine Combustion Network (ECN) injector. Additionally, all three works modeled vapor generation using the homogeneous relaxation model (HRM). The work of Moulai et al. showed that the counterbore experiences a pressure depression which may aid in expanding the fuel vapor. The work of Saha et al. included the effects of fuel evaporation due to the hot atmospheric gas. The work of Strek et al. used high fidelity x-ray tomography measurements to modify the inlet corner radius, hole and counterbore length, diameter, and convergence/divergence. Hole-to-hole mass flow rate and density profiles were then compared with x-ray tomography data to investigate the influence of manufacturing imperfections on GDI sprays. It should be noted that the solver used by Saha et al. is formulated like a sharp interface VOF model, however, in their work they deactivated the piecewise-linear interface calculation and high-resolution interface capturing schemes, and thus rendered it a diffuse interface model. The application of these methods to GDI spray simulations is still relatively new and further experimental validation will occur in future works.

The focus of the present work is the influence of transient needle motion on GDI injection. This is a novel study in the application of GDI, though it has been done before in diesel simulations. For instance, in 2014 Battistoni et al. studied the effect of off-axis needle motion on diesel DI injectors [33]. Here they found that off-axis needle motion affects hole-to-hole variation in mass flow rate as well as flow characteristics in the sac region and the orifices. The work of Battistoni et al. was conducted on a micro-sac diesel injector which has significantly greater needle lift and wobble as compared to the typical VCO GDI injector.

In the present work a computational study was performed to investigate the influence of transient needle motion on internal nozzle flow and near-nozzle sprays for gasoline direct injection. Both flashing and non-flashing conditions are simulated. Grid resolution within the nozzle holes and sac of the injector is significantly higher in this study than in the previous diffuse interface GDI studies mentioned above. This has allowed for excellent qualitative agreement with experiment and quantitative agreement with experimental rate of injection, and it has elucidated the complex internal flow which is behind perturbations and oscillations in spray angle

and mass flow rate.

Model Description

The solver used in this study was developed at the University of Massachusetts [34–38] using the foam-extend community driven extension of the OpenFOAM [39] CFD libraries. The use of these libraries provides a well parallelized code with intrinsic polyhedral mesh support, as well as access to a wide variety of RANS and LES turbulence models and a multitude of pre and post processing utilities. The code has been well validated in many prior publications in applications ranging from channel flow [35], condensing two-phase injector flow [40], cavitating diesel flows [41], and flash-boiling GDI flow [1, 31].

The governing equations of conservation of mass and momentum are solved using a single continuous velocity which represents the density averaged fields.

$$\frac{\partial \rho}{\partial t} + \nabla.\phi = 0, \tag{2}$$

$$\frac{\partial \rho \vec{U}}{\partial t} + \nabla.\left(\phi \vec{U}\right) = -\nabla p + \nabla \overline{\overline{\tau}}, \tag{3}$$

Here ϕ is the face valued mass flux and $\overline{\overline{\tau}}$ is the stress tensor accounting for viscous and turbulent effects.

A transport equation for the mean non-condensable gas mass fraction is solved to account for the mixing of the fuel with the ambient gas. This is seen in Eqn. (4).

$$\frac{\partial \rho \tilde{Y}}{\partial t} + \nabla.\left(\phi \tilde{Y}\right) = \nabla.\left(\rho \widetilde{u'Y'}\right) \tag{4}$$

The turbulent diffusion gas flux term, $\widetilde{u'Y'}$, accounts for the mixing effect of the relative velocity between the two phases. This term is closed through Fick's law of diffusion, as shown in Eqn. (5).

$$\rho \widetilde{u'Y'} = \frac{\mu_t}{Sc_r} \nabla \tilde{Y} \tag{5}$$

Here μ_t is the turbulent viscosity, and Sc_r is the realizable Schmidt number field. This field acts in the place of the typical uniform valued Schmidt number of 0.9, increasing wherever necessary to prevent the turbulent diffusion gas flux term from exceeding the magnitude of the turbulent velocity fluctuations. This formulation is described in detail here [30].

The phase change of the fuel is modeled using a method developed in 1990 by Bilicki and Kestin [42]. In this work they sought to capture the one-dimensional variability in the vapor generation and condensation rate by the addition of a partial differential equation to the homogeneous equilibrium model (HEM), calling it the homogeneous relaxation model. This additional partial differential equation governs the local and instantaneous rate that the dryness fraction tends toward its equilibrium value, taking the form,

$$\frac{Dx}{Dt} = \frac{\bar{x} - x}{\Theta} \tag{6}$$

where x is the quality, $\bar{x}$ is the equilibrium quality, and Θ is the timescale. The equilibrium quality is determined by the enthalpy and the saturated liquid and saturated vapor enthalpies at the local pressure using a lookup Table generated with the REFPROP database [43].

The timescale, Θ, is determined by an empirical fit to experimental data of flash-boiling water in pipes generated by Downar-Zapolski et al. [44]. For upstream pressures above 1 MPa, the empirical fit takes the form seen in Eqn. (7).

$$\Theta = \Theta_0 \alpha^a \phi^b \tag{7}$$

Where $\Theta_0 = 3.84 \cdot 10^{-7}$[s], α is the fuel void fraction, $a = -0.54$, $b = -1.76$, and ϕ is a dimensionless pressure defined by Eqn. (8).

$$\phi = \left|\frac{p_{sat} - p}{p_c - p_{sat}}\right| \tag{8}$$

Here p_c is the critical pressure of the fluid.

$$\begin{aligned} \frac{D\rho}{Dt} = & \left.\frac{\partial \rho}{\partial p}\right|_{x,h,y} \frac{Dp}{Dt} + \left.\frac{\partial \rho}{\partial x}\right|_{p,h,y} \frac{Dx}{Dt} \\ & + \left.\frac{\partial \rho}{\partial h}\right|_{p,x,y} \frac{Dh}{Dt} + \left.\frac{\partial \rho}{\partial y}\right|_{p,h,x} \frac{Dy}{Dt} \end{aligned} \tag{9}$$

While HRM was originally developed for one dimensional analysis, it was extended to a three-dimensional CFD model in 2010 by Schmidt et al. [35]. The introduction of variable rate phase change required a method for connecting predicted phase change with conservation of mass and momentum; the chain rule was used in the form seen in Eqn. (9). This allows for the pressure to respond to both compressibility, density change from phase change, and density change from turbulent mixing with the non-condensable gas.

Case Setup

The simulations conducted for this study were based upon the engine combustion network (ECN) spray G and spray G2 operating conditions described in Table 1. The spray G condition is non-flashing due to its elevated back pressure and the spray G2 is mildly flashing. Both conditions contain

Table 1. Non-flashing (spray G) and Flashing (spray G2) operating conditions defined by the ECN [45].

	Spray G	Spray G2
Fuel	Iso-octane	Iso-octane
Upstream Pressure	20 MPa	20 MPa
Fuel Temperature	90°C	90°C
Ambient Temperature	300°C	60°C
Ambient Density	3.5 kg/m^3	0.5 kg/m^3
Back Pressure	600 kPa	50 kPa
Injection Duration	780μs	780μs

hot fuel and therefore any vapor generation within the nozzle will occur through flash-boiling.

The mesh was based upon the nominal geometry and contained a 9 mm diameter outlet plenum. This is an 8 hole VCO injector with 5 needle guides. The nominal geometry is symmetric across the xz-plane as can be seen in Figure 1.

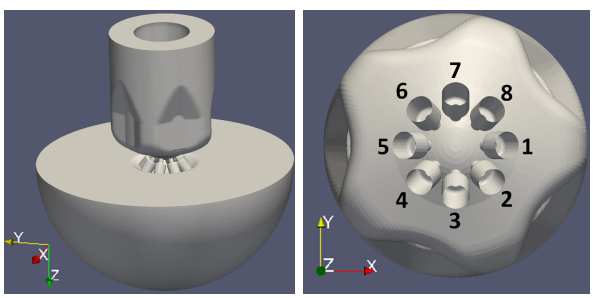

Figure 1. Nominal spray G nozzle geometry with 8 nozzle holes and 5 needle guides. Simulated domain includes 9 mm diameter outlet plenum. Hole numbering and axes orientation based upon ECN convention [45].

The total cell count was 1.44 million with a minimum cell size of 7 μm. No grid independence study was conducted, however, the cell count is comparable to or higher than that of other diffuse interface simulations reported in literature [31, 32]. Furthermore, the mesh is significantly better resolved within the sac and nozzle hole regions than these studies; the grid spacing is roughly 10 μm and 7 μm in the sac and nozzle holes respectively, compared with the 35 μm and 17.5 μm reported by Saha et. al. [32], and 40 μm and 10 μm reported by Moulai et. al. [31]. Both of these works conducted a ROI based grid independence study.

The mesh was generated using GridPro meshing software which produced a high quality mesh and allowed for anisotropic refinement in the narrow 5 μm channel between the needle and the nozzle wall. This can be observed in Figure 2. Without anisotropic refinement, the cell count for this mesh would be closer to 18 million, with most of the cells located within the 5 μm narrow channel.

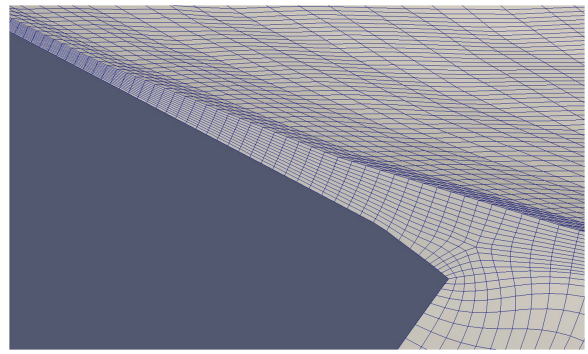

Figure 2. Cut plane of CFD mesh showing anisotropic refinement in the narrow region between the needle and the nozzle.

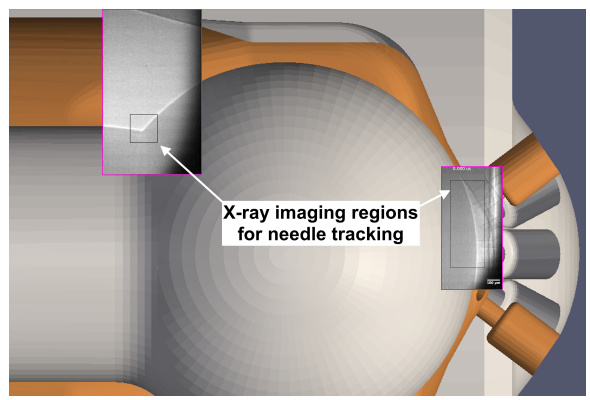

Figure 3. Cutaway of Spray G injector nominal geometry, with x-ray imaging regions overlaid.

A realistic three-dimensional needle motion profile has been applied in the simulations from measurements made via time-resolved x-ray phase contrast imaging. The experiments were conducted at the 32-ID beamline of the Advanced Photon Source (APS) at Argonne National Laboratory [46]. The injector was placed in a pressurized chamber fitted with x-ray transparent windows. A polychromatic x-ray beam was passed through the nozzle, and the internal components of the injector were imaged on a scintillator screen, which was recorded using a conventional high-speed camera and 10× microscope with a spatial resolution of 1.9 μm/pixel and

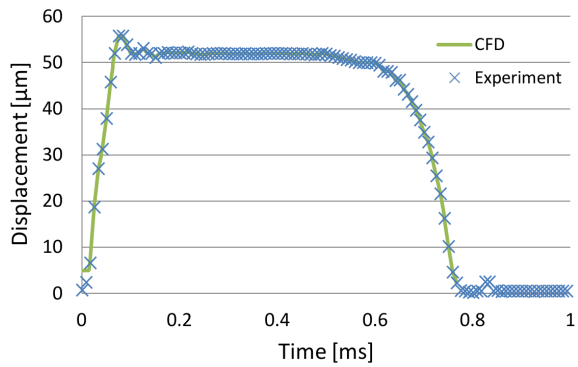

Figure 4. Ensemble-averaged needle lift (z-axis) profile from the x-ray data (blue Xs) and the lift profile used in the CFD simulations (green line). Notice the CFD profile starts at 5 μm of lift.

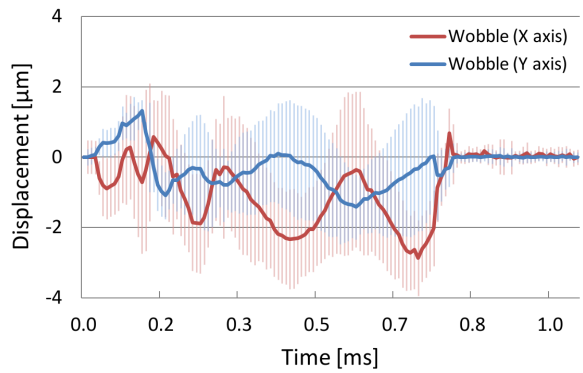

Figure 5. Ensemble-averaged needle wobble profile with 86% confidence interval bars.

a temporal resolution of 8.33 μs. Further details regarding the experiment setup may be found in prior work [47–50]. The motion of the needle was recorded at two orientations of the injector in two regions at the front and back of the check ball, as shown in Figure 3. From 30 realizations of the needle motion at each location and orientation, the ensemble average three-dimensional motions were calculated using an image correlation algorithm.

The ensemble average needle lift and off-axis wobble profiles are shown in Figures 4-5 respectively, using the ECN coordinate convention [45]. It can be seen that the needle wobbles in both the x and y directions, and at the same frequency. This means that the needle is oscillating predominantly in one direction, an observation which has previously been made in diesel injectors [17]. These oscillations are thought to be purely mechanical in diesel injectors [51], thus, it is likely that the oscillations seen here are also purely mechanical in nature.

Since the simulations require a finite positive initial needle lift, the motion used in the simulations was modified accordingly. The needle position started at 5 μm of lift and remained stationary until 14 μs into the simulation. The time of 14 μs was chosen because this was the amount of time the experimental data indicated it would take to reach 5 μm of lift. After this point, the needle position followed the experimental lift and wobble profile generated by the experiment. The internal mesh moved with Laplacian smoothing. To isolate the effects of the needle wobble, simulations were also done only with lift.

The inlet boundary was modeled using a zero gradient boundary condition for velocity and a total pressure boundary condition for pressure. The walls were modeled as no-slip with standard log-layer wall functions for the turbulence model. The outlet was modeled as zero gradient for velocity and a custom transonic total pressure condition was used for pressure. Because the outlet velocities can be supersonic, a total pressure boundary condition is not appropriate. The transonic total pressure condition smoothly transitions from total pressure to zero gradient depending on the Mach number. This boundary condition increased the stability of the simulations.

As seen in Figure 6, the internal pressure field was initialized using a hyperbolic tangent to drop the pressure in the seat region. The internal field for the non-condensable gas to fuel interface was set at the plane of minimum needle clearance.

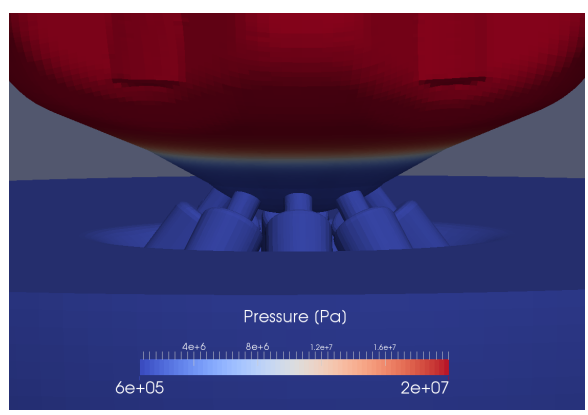

Figure 6. Pressure initial condition set with hyperbolic tangent.

Setting the internal fields in this way prevents spurious pressure waves from dominating the beginning portion of the simulation. It also allows for the

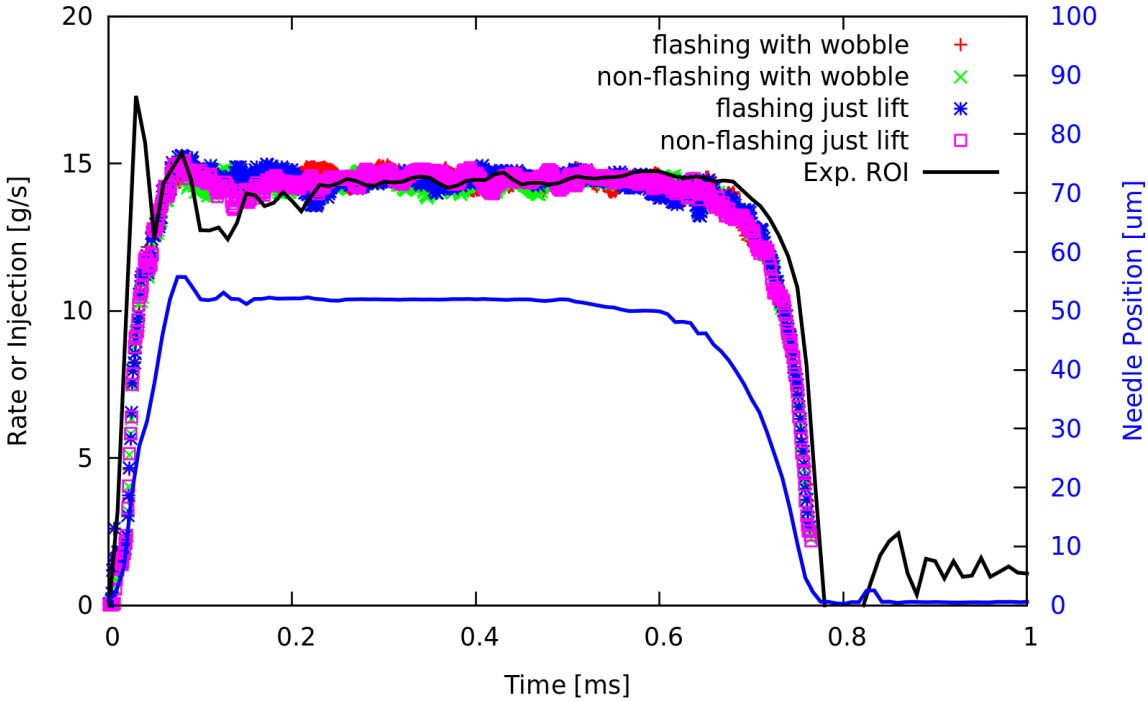

Figure 7. Simulated and experimental ROI with needle position vs. time. Experimental ROI obtained through the long-tube method and simulation ROI taken at the nozzle exit.

initial density field to be calculated appropriately, so that the fuel begins with its compressed density of 646 kg/m^3. A comparable simulation which starts with the downstream pressure throughout the domain would result in an initial equilibrium fuel density of 632 kg/m^3, and much of the simulation would include unwanted effects related to the solver working to compress the upstream fuel.

Turbulence was modeled using the SST k-ω RANS model. Compressibility of the fluid was a volume weighted average of the compressibility of the three phases, where gas and vapor compressibility were based upon the ideal gas law, and liquid compressibility was assumed to be linear. The simulation was assumed to be isenthalpic. Throttling processes are often considered isenthalpic, since no work is done by the fluid.

Results

Rate of Injection

As seen in Figure 7, the experimental rate of injection profile was captured very accurately in these simulations. The only significant differences between simulation and experiment are in the early portion of the injection where there is noise observed in the experimental data. This noise is likely due to vibrations in the experimental rig [51]. The simulated rate of injection follows the needle lift profile, even responding to the transient overshoot which occurs just as the needle is reaching peak lift. This result shows that an accurate rate of injection profile can be obtained through CFD simulations with pressure boundary conditions and transient needle motion to actuate injection.

Qualitative Validation

The qualitative behavior of these simulations matches well with experiment in three ways. First, the results for the non-flashing spray G condition predicted ingestion of ambient gas into the nozzle counter-bores. In contrast to this, the flashing spray G2 condition predicted no ingestion of ambient gas. As seen in Figure 8, experimental imaging of flashing and non-flashing GDI injection has shown the same behavior.

Next, our simulations predicted an expansion and perturbation of spray angle at the end of injection. This has been observed through experimental imaging as seen in Figure 9 where the liquid mass fraction is compared with experimental images in the non-flashing condition.

Finally, when comparing a simulated animation to experimental footage, it was found that the fre-

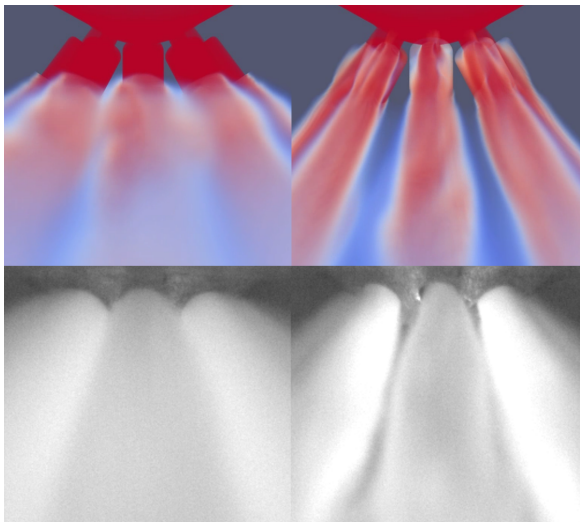

Figure 8. Flashing (left) and non-flashing (right) experimental images (bottom) and volume rendered fuel mass fraction from CFD (top). Uniform contact of fuel with counter-bore is seen under flashing conditions, while non-flashing shows gaps in contact allowing ingestion of ambient gas.

quency of the oscillations in the spray plumes match very well. These oscillations in the spray plumes were found to be the result of unsteady flow within the sac influencing the flow characteristics within the 8 holes. This idea is explored more later in this section.

Flash-boiling at Low Lift Conditions

At low needle lift conditions at the end of injection, very low pressures occur within the injector in the narrow region between the needle and the nozzle wall. This causes fuel vapor to be generated as fuel rushes past the needle, see Figure 10. This vapor generation may influence the post-injection condition of the sac, with the inevitable vapor collapse aiding in the ingestion of ambient gas. Furthermore, it is possible that cold fuel may cavitate in this region of the nozzle, potentially damaging the nozzle walls over time.

Needle Wobble

Simulations were conducted with and without needle wobble to help isolate any influence the lateral motion of the needle may have on the spray. The variation in hole-to-hole mass flow rate was compared with needle wobble, however no significant correlation could be found. These variations instead appear to be somewhat random and displayed little to no symmetry across the x-z plane.

This was a somewhat unexpected result as pre-

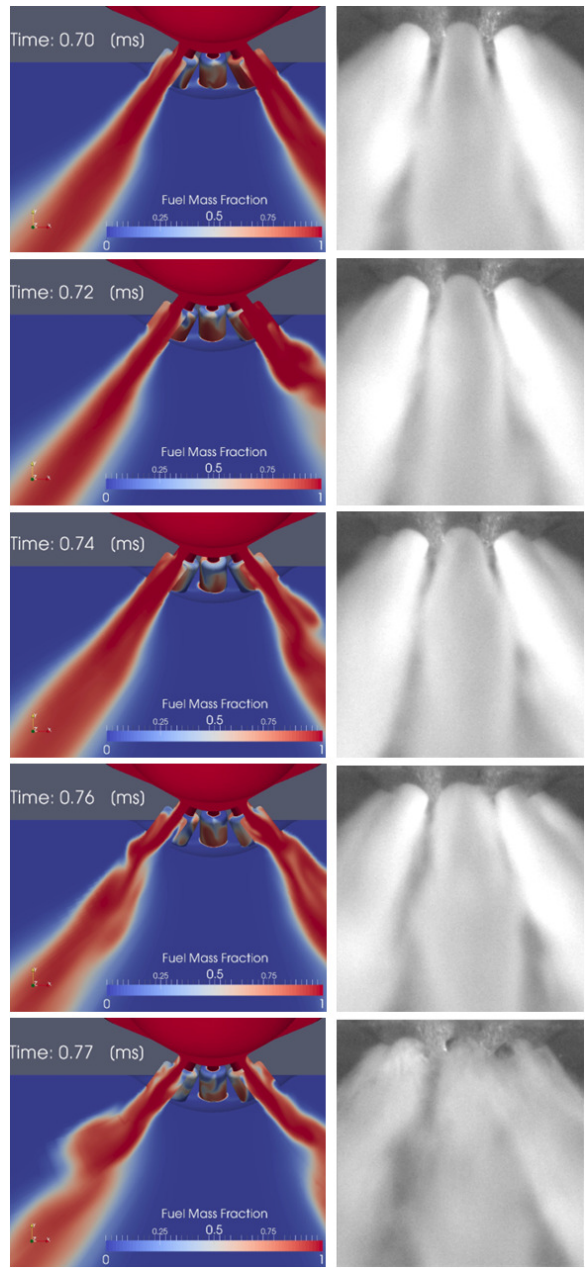

Figure 9. Simulated fuel mass fraction compared with experimental imaging at the end of non-flashing simulation. Note that the spray angle increases as flow is disrupted with the closing of the needle.

vious works have shown that needle wobble can influence spray structure in diesel injectors [33]. It is not, however, unexplainable as the spray G geometry differs significantly from that of a diesel injector. First of all, the magnitude of the lift and wobble are significantly less for GDI injectors. This means that needle velocities are lower, with a peak wob-

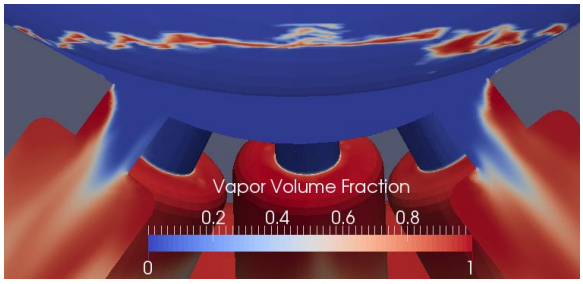

Figure 10. Vapor generated at low lift conditions near the end of injection.

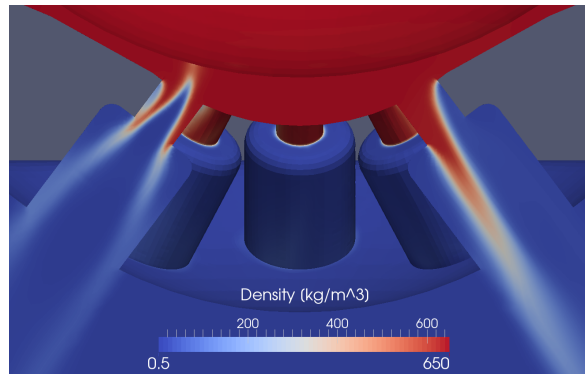

Figure 11. Density field reveals the influence of vapor generation at the inlet corner of the nozzle holes. The left hole is also generating vapor through string flash-boiling.

ble velocity of less than 0.2 m/s in this case. Next, the needle has a spherical tip. This means that the bottom portion of the needle surface is close to parallel to any wobble motion, and thus wobble does not displace any significant volume of fluid in the nozzle sac. Finally, the magnitude of the wobble is small, around 3 μm. This small and slow wobble results in its most significant displacement of volume far upstream of the nozzle holes, and any influence this motion has on the flow is far overshadowed by the highly turbulent and complex flow which follows further downstream.

Complex Internal Flow

As fuel moves past the needle it accelerates to roughly 140 m/s. Upon reaching the location of the nozzle holes it then either enters a nozzle hole or the nozzle sac. The sac flow contains many transient and interacting vortices which are continuously being driven in all directions by the high speed upstream flow as well as the 8 low pressure sinks provided by the nozzle holes. The result is a complex internal flow which produces hole-to-hole fluctuations in mass flow rate, slight oscillations and variation of the spray angle, consistent flash-boiling at the inlet corner of the nozzle holes, and intermittent string flash-boiling as vortices are entrained into the nozzle holes. Each of these features will be assessed in more detail within this section.

First, the inlet corners of each of the 8 nozzle holes consistently produces a pressure drop adequate enough to generate substantial amounts of fuel vapor. As can be seen in Figure 11, this occurs on the upstream side of the nozzle holes. Here high velocity fuel encounters the hole and a huge pressure drop results as the momentum of the fuel prevents it from following the sharp feature. Vapor generation here is aided by the fact that this simulation was conducted on the nominal geometry which contains sharp inlet corners.

Next, the flow in the injector sac contains many transient and interacting vortices. These vortices are generated as high speed flow enters the sac from all directions and encounters a strong adverse pressure gradient. The low pressure regions of the nozzle holes continuously pull on the flow, inducing swirl and providing sinks into which the vortices drain. Three types of vortices were commonly observed in these simulations and they can be seen in Figures 12-14.

- **Type 1:** A vortex which simultaneously drains into two adjacent nozzle holes. The streamlines on Figures 12 and 13 help show how this happens; the vortex is fed from the bottom by flow directly upstream of the vortex and fed from the top by sac flow. As the sac flow encounters upstream flow their momentum relative to the nozzle holes cancel out resulting in a vortex which then simultaneously drains into both holes. This type of vortex is semi-stable, typically lasting on the order of 10-20 μs.

- **Type 2:** A vortex which drains into a single nozzle hole, with the other end terminating on the needle of the injector. This is seen in Figure 14. These vortices are fed primarily by upstream flow and they are significantly more stable, lasting on the order of 40-80 μs.

- **Type 3:** A vortex which does not feed into a nozzle hole, terminating on the nozzle wall and the bottom of the needle. This can be seen in the right center of Figure 12. Such a vortex typically either dissipates within 5-10 μs or migrates to a nozzle hole and is re-energized.

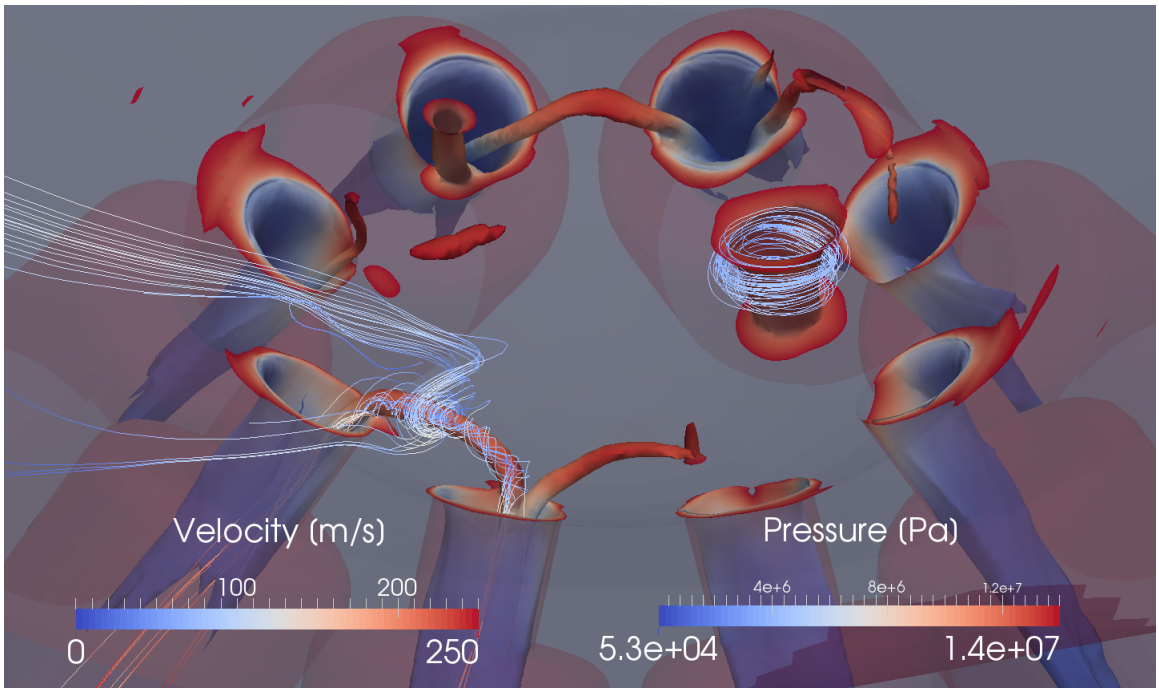

Figure 12. Isosurface of 14 MPa total pressure colored by static pressure with velocity streamlines colored velocity magnitude. Vorticies contained in the sac can be seen to terminate on a wall or they can be entrained into one or two nozzle holes.

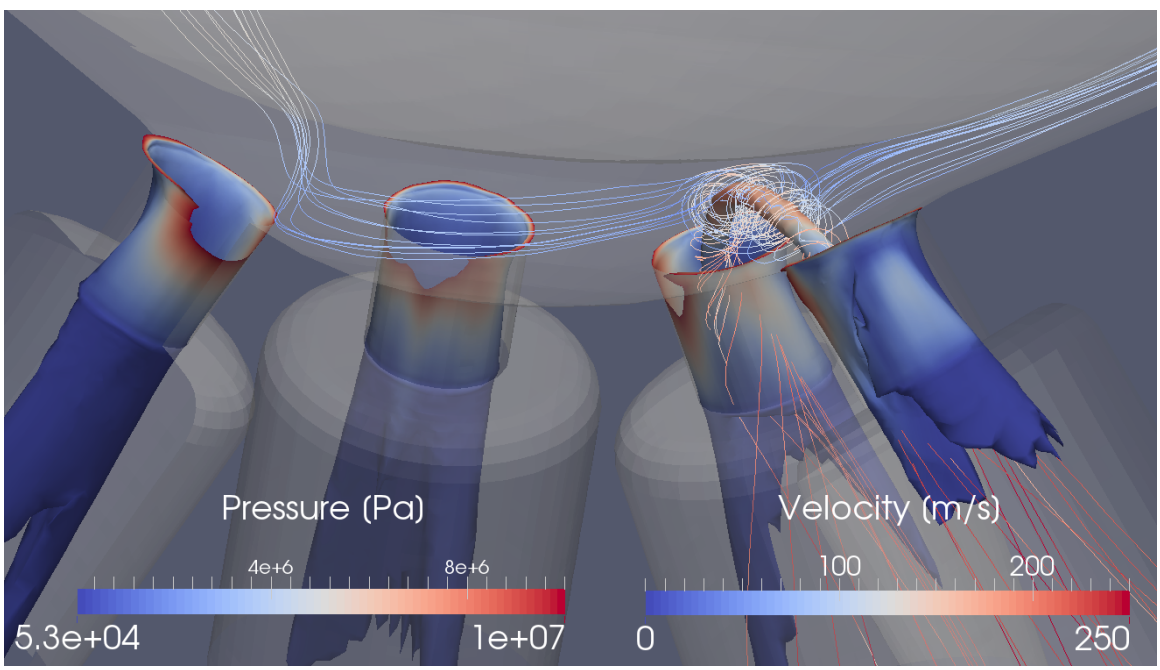

Figure 13. Isosurface of 10 MPa total pressure colored by static pressure with velocity streamlines colored velocity magnitude.

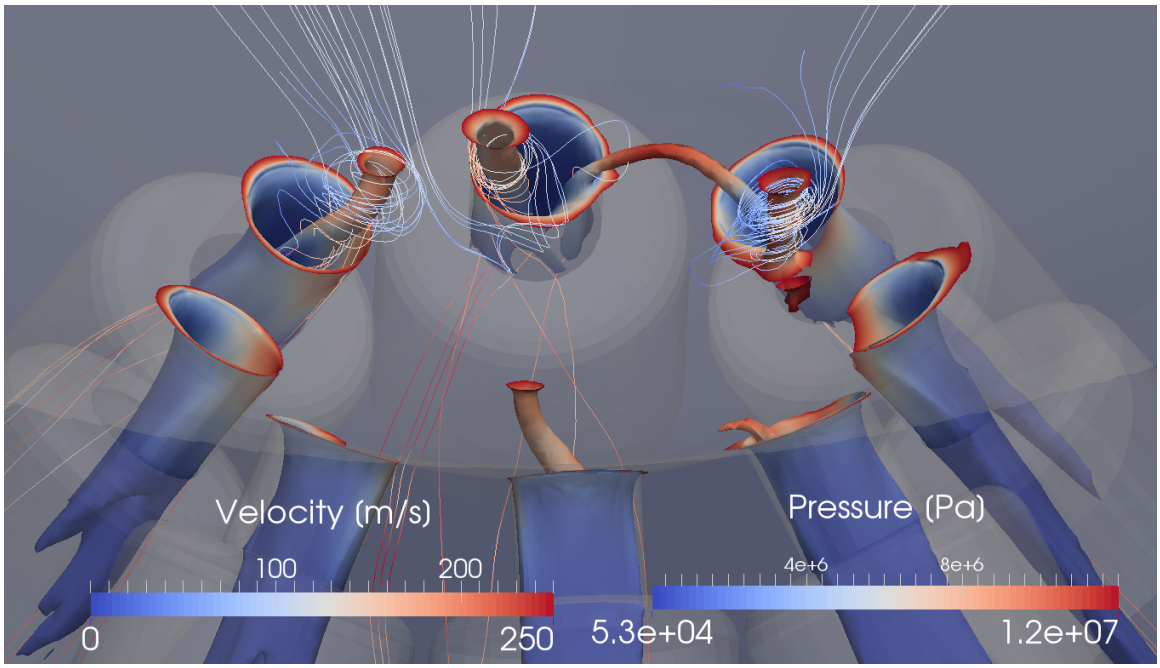

Figure 14. Isosurface of 12 MPa total pressure colored by static pressure with velocity streamlines colored velocity magnitude.

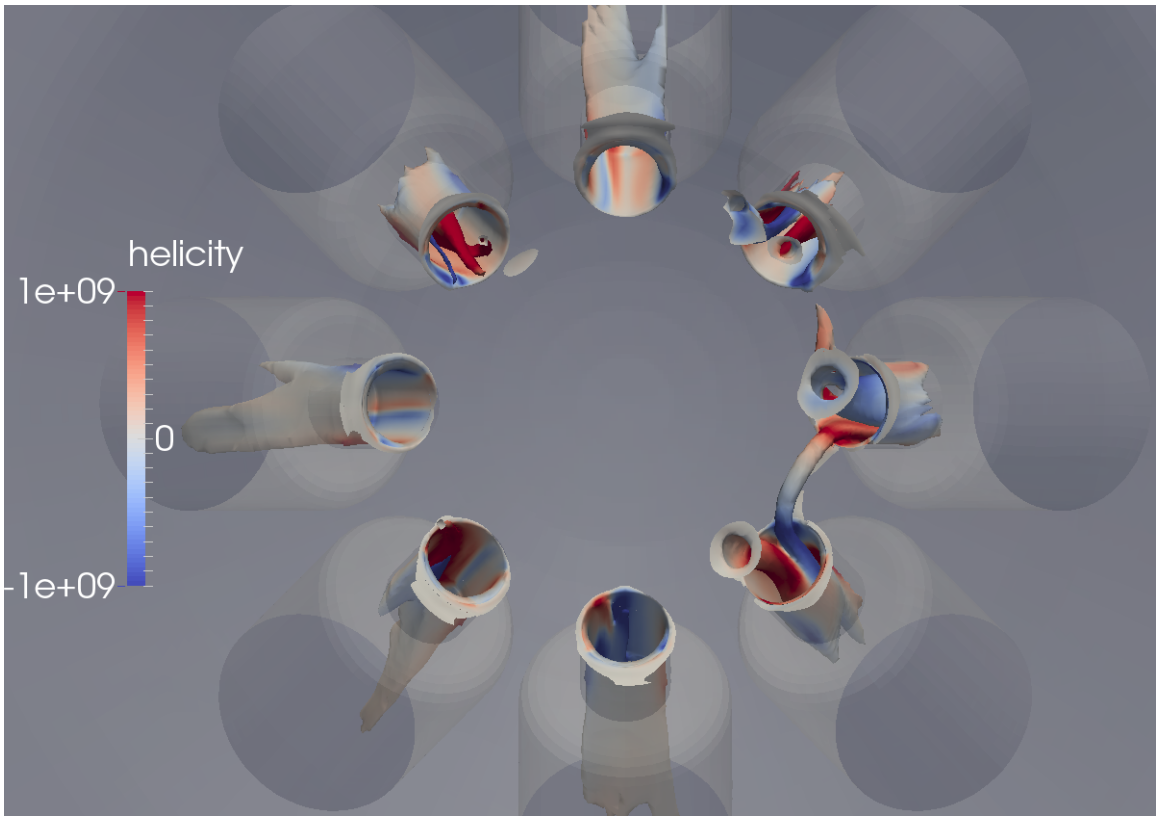

Figure 15. Isosurface of 14 MPa total pressure colored by helicity. This figure reveals that counter-rotating vortices often drain into the same nozzle hole.

The estimated timescales of these vortices were generated from animations of total pressure isosurfaces. It is common for vortices to move around, merge together, and/or split apart, thus transitioning sequentially from type to type.

The behavior of these vortices can be understood more with the help of examination of the helicity of the flow. Helicity is the dot product of the velocity with the vorticity. Thus, it is a signed scalar field which can be useful in determining the direction of the flow rotation. As seen in Figure 15, it is common for two counter-rotating vortices to drain into a single nozzle hole. Co-rotating vortices, on the other hand are unstable and tend to either merge together or break each other apart.

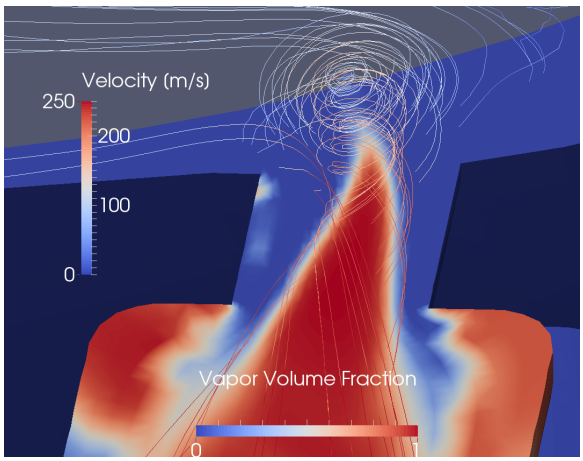

Figure 16. String flash boiling resulting from the swirling flow in the sac. Streamlines are colored by velocity and the cut plane is colored by the vapor volume fraction.

As vortices are entrained into the nozzle holes, the simulation predicts vapor generation through string flash-boiling in the center of these vortices. This string flash-boiling can be seen in Figures 16 and 17 where a single vortex, or two counter-rotating vortices can result in a significant drop in flow density. The swirling nature of the flow also has an influence on the vapor generated at the inlet corner as seen in Figure 17.

The complex internal nozzle flow ultimately results in oscillations of the mass flow rate and perturbations and expansions of the spray angle. Figure 18 shows the expansion of the spray angle caused by string flash-boiling where the nozzle on the left contains a large vortex and the hole on the right does not.

The mass flow rate and averaged density were

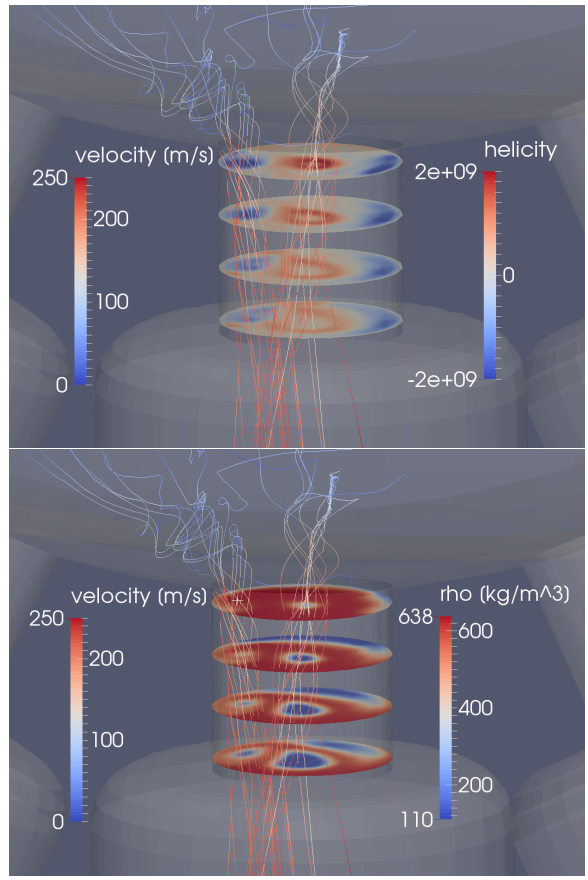

Figure 17. Two counter-rotating vortices being entrained into a single nozzle hole. Streamlines are colored by velocity and the cut planes are colored by helicity on the top image and density on the bottom image.

calculated across cute planes perpendicular to individual nozzle holes and the results are shown in Figure 19. The oscillations in the average density are due to the vapor generation at the inlet corner and through string flash-boiling. These oscillations clearly influence the nozzle hole ROI.

Conclusions

Spray G flashing and non-flashing injection has been simulated with transient needle motion. The primary results are summarized below:

- The results demonstrate the ability of CFD simulations to capture the rate of injection by prescribing the upstream pressure and lifting the needle using dynamic mesh motion. The use of a hyperbolic tangent function to set the initial pressure condition was helpful in preventing large pressure waves in the system.

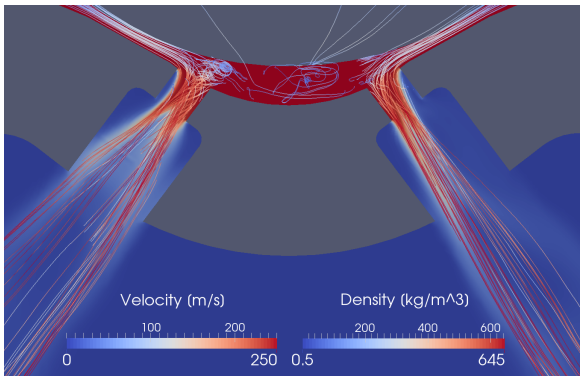

Figure 18. The expansion of the spray angle caused by string flash-boiling. Streamlines are colored by velocity magnitude and the cut plane is colored by density.

- The results were quantitatively validated against experimental imaging, capturing spray angle expansion and perturbation due to the closing of the needle, predicting the presence or lack of ambient gas ingestion into the counterbore, and capturing the oscillation frequency in the spray plumes.
- At low lift conditions vapor generation is observed in the seat area as the fuel flows past the narrow region of the needle.
- Needle wobble is shown to have no measurable influence on the hole-to-hole variation in mass flow rate and spray structure.
- The complex flow contained within the fuel injector sac is analyzed and shown to contain transient interacting vortices which result in string flash-boiling, perturbations in spray angle and direction, and oscillations in mass flow rate.
- The oscillations in mass flow rate are ultimately attributed to the presence of vapor within the nozzle holes decreasing the average flow density.

Future work will include a comparison to experimental x-ray tomography data for downstream mass distribution and comparison to flow through an as-built geometry.

Acknowledgements

The authors would like to acknowledge the financial support of General Motors, who has sponsored much of the development of this CFD solver.

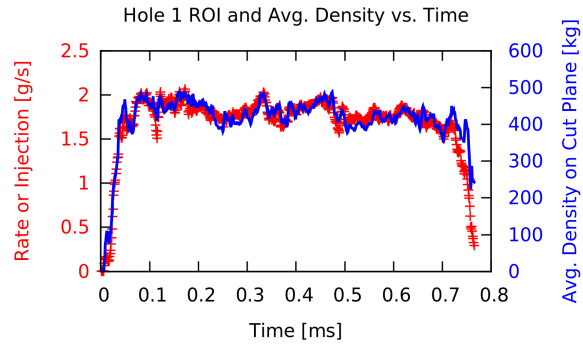

Figure 19. Rate of injection and average density across hole 1 cut plane.

The mesh used in these simulations was generated using GridPro meshing software. The authors gratefully acknowledge the assistance provided by GridPro in helping to exploit their tool to generate such a complex grid.

The x-ray needle lift experiments were performed at the 32-ID beam line of the APS at Argonne National Laboratory. Use of the APS is supported by the U.S. Department of Energy (DOE) under Contract No. DE-AC02- 06CH11357. Argonne's fuel spray research is sponsored by the DOE Vehicle Technologies Program, under the direction of Gurpreet Singh and Leo Breton.

References

[1] Piotr Strek, David Schmidt, and Daniel Duke. SAE 2016 World Congress & Exhibition, Detroit, MI, 2016.

[2] Matthew Blessinger, Julien Manin, Scott A. Skeen, Maarten Meijer, Scott Parrish, and Lyle M. Pickett. International Journal of Engine Research, 16(2):238–252, 2015.

[3] Kshitij Deepak Neroorkar. Phd, University of Massachusetts - Amherst, 2011.

[4] Lucio Postrioti, Maurizio Bosi, Andrea Cavicchi, Fakhry AbuZahra, Rita Di Gioia, and Giovanni Bonandrini. Momentum Flux Measurement on Single-Hole GDI Injector under Flash-Boiling Condition. Technical Report 2015-24-2480, SAE, 2015.

[5] Eran Sher, Tali Bar-Kohany, and Alexander Rashkovan. Progress in Energy and Combustion Science, 34(4):417–439, 2008.

[6] Min Xu, Yuyin Zhang, Wei Zeng, Gaoming Zhang, and Ming Zhang. SAE Int. J. Fuels Lubr., 6(1):137–148, 2013.

[7] Wei Zeng, Min Xu, Ming Zhang, Yuyin Zhang, and David J. Cleary. Experimental Thermal and Fluid Science, 40:81–92, 2012.

[8] Wei Zeng, Min Xu, Gaoming Zhang, Yuyin Zhang, and David J. Cleary. Fuel, 95:287–297, 2012.

[9] Gaomimg Zhang, Min Xu, Yuyin Zhang, Ming Zhang, and David J. Cleary. Atomization and Sprays, 23(3):265–278, 2013.

[10] P. G. Aleiferis and Z. R. Van Romunde. Fuel, 105:143–168, 2013.

[11] Z. Van Romunde and P.G. Aleiferis. Atomization and Sprays, 19(3):207–234, 2009.

[12] Scott E. Parrish, R. J. Zink, Y. Sivathanu, and J. Lim. ILASS Americas, 22nd Annual Conference on Liquid Atomization and Spray Systems, 2010.

[13] J. Serras-Pereira, Z. Van Romunde, P. G. Aleiferis, D. Richardson, S. Wallace, and R. F. Cracknell. Fuel, 89(9):2592–2607, 2010.

[14] Gele Aori, David L.S. Hung, Ming Zhang, Gaoming Zhang, and Tianyun Li. Atomization and Sprays, 26(5):439–462, 2016.

[15] R.D. Oza and J.F. Sinnamon. An experimental and analytical study of flash-boiling fuel injection. Technical Report 830590, SAE, 1983.

[16] S. Negro and G. M. Bianchi. International Journal of Thermal Sciences, 50(8):1460–1471, 2011.

[17] Alan L. Kastengren, F Zak Tilocco, Christopher F Powell, Julien Manin, Lyle M Pickett, Raúl Payri, Tim Bazyn, C M T Motores Termicos, and Universitat Politecnica De Valencia. Atomization and Sprays, 22(12):1011–1052, 2012.

[18] Ming Zhang, Michael C. Drake, and Kevin Peterson. Proceedings of the ASME 2013 Internal Combustion Engine Division Fall Technical Conference, Dearborn, Michigan, 2013.

[19] Q. Xue, M. Battistoni, C.F. Powell, D.E. Longman, S.P. Quan, E. Pomraning, P.K. Senecal, D.P. Schmidt, and S. Som. International Journal of Multiphase Flow, 70:77–88, 2015.

[20] Mark A. Shost, Ming-Chia Lai, Bizhan Befrui, Peter Spiekermann, and Daniel L. Varble. GDi Nozzle Parameter Studies Using LES and Spray Imaging Methods. Technical Report 2014-01-1434, SAE, 2014.

[21] Bizhan Befrui, Giovanni Corbinelli, Peter Spiekermann, Mark Shost, and Ming-Chia Lai. SAE Int. J. Fuels Lubr., 5(2):620–636, 2012.

[22] Rainer N. Dahms, Julien Manin, Lyle M. Pickett, and Joseph C. Oefelein. Proceedings of the Combustion Institute, 34(1):1667–1675, jan 2013.

[23] Rainer N. Dahms and Joseph C. Oefelein. Physics of Fluids, 25(9), 2013.

[24] A. Vallet, A. A. Burluka, and R. Borghi. Atomization and Sprays, 11:619–642, 2001.

[25] Wei Ning, Rolf D. Reitz, Ramachandra Diwakar, and Andreas M. Lippert. Atomization and Sprays, 19(8):727–739, 2009.

[26] Qingluan Xue, Michele Battistoni, Sibendu Som, Shaoping Quan, P. K. Senecal, Eric Pomraning, and David P. Schmidt. SAE International Journal of Engines, 7(2), 2014.

[27] José María Desantes, Raúl Payri, Jaime Gimeno, and Pedro Marti-Aldaravi. Simulation of the First Millimeters of the Diesel Spray by an Eulerian Spray Atomization Model Applied on ECN Spray A Injector. Technical Report 2014-01-1418, SAE, 2014.

[28] Francisco Javier Salvador, Jaime Gimeno, José Manuel Pastor, and Pedro Martí-Aldaraví. International Journal of Multiphase Flow, 65:108–116, 2014.

[29] Jose M Garcia-Oliver, Jose M. Pastor, A. Pandal, N. Trask, E. Baldwin, and David P. Schmidt. Atomization and Sprays, 23(1):71–95, 2013.

[30] J. M. Desantes, J. M. Garcia-Oliver, J. M. Pastor, A. Pandal, E. Baldwin, and D. P. Schmidt. International Journal of Multiphase Flow, 80:89–99, 2016.

[31] Maryam Moulai, Ronald Grover, Scott Parrish, and David Schmidt. Internal and Near-Nozzle Flow in a Multi-Hole Gasoline Injector Under Flashing and Non-Flashing Conditions. Technical Report 2015-01-0944, SAE, 2015.

[32] Kaushik Saha, Sibendu Som, Michele Battistoni, Yanheng Li, S. Quan, and P. K. Senecal. Proceedings of the ASME 2015 Internal Combustion Engine Division Fall Technical Conference, 2015.

[33] Michele Battistoni, Qingluan Xue, Sibendu Som, and Eric Pomraning. SAE Int. J. Fuels Lubr., 7(1):167–181, 2014.

[34] S. Gopalakrishnan and D. Schmidt. SAE Int. J. Engines, 1(1):160–170, 2009.

[35] David P. Schmidt, S. Gopalakrishnan, and H. Jasak. International Journal of Multiphase Flow, 36(4):284–292, 2010.

[36] K. Neroorkar, B. Shields, R. Grover, Jr., A. Plazas Torres, and D.P. Schmidt. Application of the Homogeneous Relaxation Model to Simulating Cavitating Flow of a Diesel Fuel. Technical Report 2012-01-1269, SAE, 2012.

[37] K. Neroorkar and D.P. Schmidt. A Computational Investigation of Flash-Boiling Multi-hole Injectors with Gasoline-Ethanol Blends. Technical Report 2011-01-0384, SAE, 2011.

[38] K. Neroorkar and David P. Schmidt. Fuel, 90(2):665–673, 2011.

[39] H.G. Weller, G. Tabor, H. Jasak, and C. Fureby. Computers in Physics, 12(6):620, 1998.

[40] Michael Colarossi, Nathaniel Trask, David P. Schmidt, and Mark J. Bergander. International Journal of Refrigeration, 35(2):290–299, 2012.

[41] Daniel J. Duke, Andrew Swantek, Zak Tilocco, Alan L. Kastengren, Kamel Fezzaa, Kshitij Neroorkar, Maryam Moulai, Christopher Powell, and David P. Schmidt. SAE Int. J. Engines, 2014.

[42] Z. Bilicki and J. Kestin. Proceedings of the Royal Society A: Mathematical, Physical and Engineering Sciences, volume 428, pp. 379–397, 1990.

[43] E.W. Lemmon, M.L. Huber, and M.O. McLinden. NIST Standard Reference Database 23: Reference Fluid Thermodynamic and Transport Properties-REFPROP, Version 9.1, National Institute of Standards and Technology, Standard Reference Data Program, Gaithersburg, 2013.

[44] P. Downar-Zapolski, Z. Bilicki, L. Bolle, and J. Franco. International Journal of Multiphase Flow, 22(3):473–483, 1996.

[45] http://www.sandia.gov/ecn/index.php.

[46] Q. Shen, W-K Lee, K. Fezzaa, Y.S. Chu, F. De Carlo, P. Jemian, J. Ilavsky, M. Erdmann, and G.G. Long. Nuclear Instruments and Methods in Physics Research Section A: Accelerators, Spectrometers, Detectors and Associated Equipment, 582(1):77–79, 2007.

[47] A.L. Kastengren, C. Powell, F. Tilocco, Z. Liu, S. Moon, X. Zhang, and J. Gao. SAE Journal, pp. 2011–01–0383, 2011.

[48] C.F. Powell, A.L. Kastengren, Z. Liu, and K. Fezzaa. Journal of Engineering for Gas Turbines and Power, 133(1):012802, 2011.

[49] D.J. Duke, A.B. Swantek, Z. Tilocco, A.L. Kastengren, K. Fezzaa, K. Neroorkar, M. Moulai, C.F. Powell, and D.P. Schmidt. SAE Int. J. Engines, 7(2):1003–1016, 2014.

[50] J.P. Viera, R. Payri, A.B. Swantek, D.J. Duke, N. Sovis, A.L. Kastengren, and C.F. Powell. Energy Conversion and Management, 112(C):350–358, 2016.

[51] Julien Manin, Alan L. Kastengren, and Raúl Payri. Journal of Engineering for Gas Turbines and Power, 134(12):122801, 2012.